STM JOURNALS

Journal of
Polymer & Composites

ISSN: 2321-2810 (Online)
ISSN: 2321-8525 (Print)
Volume 14, Special Issue 2, 2026
DOI (Journal): 10.37591/JoPC

https://journals.stmjournals.com/jopc

Research JoPC

Mechanical and Thermal Performance of PETG Composites Reinforced with Short Carbon Fibers via Fused Filament Fabrication

Ananda M.N.[1,*], Sudheer Reddy J.[2]

Abstract

The study investigates the fabrication and characterization of polyethylene terephthalate glycol (PETG) composites reinforced with short carbon fibers (CF) using the fused filament fabrication (FFF) technique. Composite filaments with varying CF weight fractions (0, 5, 10, 15, and 20 wt%) were produced and evaluated for their mechanical, thermal, and morphological performance. The influence of CF reinforcement on tensile, flexural, and impact behavior was systematically examined, alongside thermal stability metrics including heat deflection temperature (HDT) and glass transition temperature (Tg). Scanning electron microscopy (SEM) was utilized to examine fiber distribution, fracture surface characteristics, and the quality of interlayer bonding. The results revealed a substantial improvement in mechanical properties with increasing CF content. Tensile strength improved from ~51 MPa (neat PETG) to ~68 MPa at 20 wt% CF, while Young's modulus increased by 60%. Flexural strength and modulus similarly rose by 44% and 76%, respectively. Thermal analysis showed a rise in HDT from 70 °C to 83 °C, and Tg increased from 81.5 °C to 83.6 °C, indicating improved heat resistance. Nevertheless, as the fiber content increased, the elongation at break declined, indicating greater brittleness. SEM images confirmed good fiber–matrix bonding up to 10 wt% CF, with agglomeration and voids emerging at higher loadings. Overall, CF-reinforced PETG composites produced via FFF demonstrate significant potential for engineering applications demanding high stiffness and thermal performance. An optimal balance between strength and processability was observed around 10-15 wt% CF. These findings offer a scalable pathway for high-performance, fiber-reinforced thermoplastics in additive manufacturing.

Keywords: PETG, carbon fiber, fused filament fabrication, mechanical properties, thermal conductivity, microstructure, composite filaments

*Author for Correspondence
Ananda M.N.

[1]Assistant Professor, Centre for Additive Manufacturing, Department of Mechanical Engineering, Nitte (Deemed to be University), Nitte Meenakshi Institute of Technology (NMIT), Bengaluru, Karnataka, India
[2]Professor, Centre for Additive Manufacturing, Department of Mechanical Engineering, Nitte (Deemed to be University), Nitte Meenakshi Institute of Technology (NMIT), Bengaluru, Karnataka, India

Received Date: August 08, 2025
Accepted Date: August 26, 2025
Published Date: February 24, 2026

Citation: Ananda M.N., Sudheer Reddy J.. Mechanical and Thermal Performance of PETG Composites Reinforced with Short Carbon Fibers via Fused Filament Fabrication. Journal of Polymer & Composites. 2026; 14(Special Issue 2): S1219–S1238p.

INTRODUCTION

Additive Manufacturing (AM) has transformed the manufacturing landscape by enabling on-demand, tool-less production of complex geometries with reduced material waste [1]. Its versatility, design freedom, and potential for rapid prototyping have positioned it as a key enabler in industries ranging from aerospace and automotive to biomedical and consumer products [2]. AM techniques are broadly categorized into several processes, including vat photopolymerization, powder bed fusion, binder jetting, material extrusion, and more each offering specific advantages based on application requirements [3–4]. Among these, Fused Filament Fabrication (FFF) a material extrusion-based technique has become

one of the most widely adopted AM technologies due to its low cost, ease of use, and compatibility with a range of thermoplastics [5–6]. In FFF, parts are fabricated layer by layer by extruding molten filament through a heated nozzle, which solidifies upon deposition. While the method is attractive for prototyping and small-batch production, its use in high-performance and load-bearing applications remains limited by the mechanical performance of the printed parts [7–8]. To improve the performance of FFF-printed components, material selection plays a crucial role. One material gaining popularity is Polyethylene Terephthalate Glycol (PETG) a semi-crystalline copolymer that combines the ease of printing of PLA with the toughness and durability of ABS. PETG exhibits low warping, good chemical resistance, high impact strength, and minimal shrinkage during printing. These properties make it an attractive candidate for FFF where dimensional stability and print reliability are critical [9-10]. Its lower tendency to absorb moisture and better UV resistance compared to PLA and ABS further extend its utility in outdoor and semi-structural applications. However, the mechanical strength of pure PETG remains insufficient for demanding structural or thermally loaded parts. A promising approach to overcoming this limitation is the incorporation of carbon fiber (CF) reinforcement [11–12]. Short carbon fibers dispersed within the PETG matrix can significantly enhance tensile strength, modulus, and thermal performance. CF reinforcement in FFF not only improves load-bearing capacity but also influences thermal conduction and reduces shrinkage-induced distortion by improving heat dissipation across layers [13–14].

Despite the growing interest in PETG-CF composites, several critical gaps exist in current research. Most studies focus on basic mechanical testing, without exploring the microstructural foundations such as fiber orientation, interfacial bonding, and void distribution that drive these performance changes. The influence of FFF-specific process parameters on fiber alignment and anisotropic mechanical response is often overlooked. Furthermore, long-term behaviors such as fatigue, interlayer bonding strength, and thermal degradation resistance have not been sufficiently addressed, limiting confidence in their structural deployment. This study aims to provide a comprehensive evaluation of short carbon fiber-reinforced PETG composites fabricated via the FFF process. The investigation focuses on mechanical, thermal, and morphological characterization, with an emphasis on the influence of CF content and printing parameters. The study incorporates tensile, thermal (TGA, DSC), and microscopy (SEM) analyses to establish a correlation between fiber reinforcement, process-induced microstructure, and performance.

MATERIALS AND METHODS

Materials

Polyetheretherketone The base polymer used in this study is Polyethylene Terephthalate Glycol (PETG), with a melt flow index (MFI) of 6.5 g/10 min (measured at 250 °C under a 2.16 kg load), and a glass transition temperature (Tg) of approximately 80 °C. PETG was selected due to its favorable balance of mechanical strength, impact resistance, and thermal stability, along with low warpage characteristics during extrusion-based additive manufacturing [15–17]. The reinforcement material consisted of short, chopped carbon fibers (SCFs) supplied by, with an average fiber length of 150300 μm and a nominal diameter of 7 μm. The materials used in this study include commercial-grade PETG pellets and short, chopped carbon fibers (SCFs). PETG, being a copolyester, exhibits lower crystallinity and enhanced toughness compared to PET. This amorphous nature facilitates uniform flow during FFF, promoting good interlayer adhesion [18–19]. However, its moderate stiffness and heat deflection temperature limit its utility in structural applications. The inclusion of carbon fibers addresses this by acting as load-bearing fillers and thermal dissipaters. According to the rule of mixtures, the composite modulus and strength increase proportionally with filler loading, provided uniform dispersion and interfacial bonding are achieved [20–21]. Short fibers in the 150–300 μm range are ideal for FFF as they minimize nozzle clogging while still contributing to reinforcement. Detailed material properties are presented in Table 1 and Table 2, respectively. The filament compounding process was performed using a laboratory-scale twin-screw extruder, the specifications of which are shown in Table 3.

Table 1. Properties of PETG base polymer [26].

Property	Value
Density	1.27 g/cm³
Melt Flow Index (250 °C, 2.16 kg)	6.5 g/10 min
Glass Transition Temperature	~80 °C
Tensile Strength	50–55 MPa
Tensile Modulus	2000 MPa
Elongation at Break	15–25%
Impact Strength (Notched Izod)	80 J/m
Supplier	Polymercrafts, Bengaluru

Table 2. Properties of short carbon fibers (SCFs) [27].

Property	Value
Average Fiber Length	150–300 µm
Fiber Diameter	~7 µm
Density	1.75 g/cm³
Tensile Strength	~3.5 GPa
Tensile Modulus	~230 GPa
Thermal Conductivity	~10 W/m·K
Electrical Conductivity	High (Anisotropic)
Supplier	Parshwa Composite, Belagavi

Table 3. Twin-screw extruder configuration [32].

Parameter	Value
Model	Thermo Scientific™ Process 11
Screw Diameter	11 mm
L/D Ratio	40:1
Temperature Zones	6
Temperature Range	230–250 °C
Screw Speed	60 rpm
Throughput	~200 g/h
Cooling System	Water Bath + Air Cooling
Output Filament Diameter	1.75 ± 0.05 mm

Figure 1. Visual representation of (a) PETG pellets and (b) Short chopped carbon fibers.

The Figure 1 illustrates the raw materials used in the fabrication of carbon fiber–reinforced PETG composites via fused filament fabrication (FFF). In Figure 1(a), PETG pellets are shown in their pre-

extrusion form cylindrical and semi-transparent highlighting their thermoplastic nature and consistent geometry, which are essential for stable extrusion and filament quality. PETG, a glycol-modified copolyester, offers excellent printability and chemical resistance, making it suitable for structural and semi-structural additive manufacturing applications. Figure 1(b) displays short carbon fibers (SCFs), which serve as reinforcement in the PETG matrix. These fibers, typically 150-300 μm in length, contribute significantly to the composite's stiffness, strength, and thermal stability. Their high aspect ratio and graphitic microstructure provide effective load transfer under mechanical stress. Furthermore, the presence of functional groups on the fiber surface enhances interfacial adhesion with the PETG matrix during compounding, thereby improving composite integrity.

To investigate the influence of carbon fiber reinforcement on the material properties of PETG composites, five distinct formulations were developed by varying the weight percentage of carbon fiber from 0% to 20% [22–25]. The corresponding PETG content was reduced proportionally to maintain a constant total weight. This compositional distribution is visually represented in Figure 2. The inclusion levels 0%, 5%, 10%, 15%, and 20% CF were strategically selected based on both processing feasibility and literature precedence. The 0 wt% sample (Sample 1) serves as the control (neat PETG), establishing baseline thermal and mechanical behavior. The 5 wt% and 10 wt% CF levels (Samples 2 and 3) represent moderate fiber loadings, typically reported to yield noticeable improvements in stiffness and thermal conductivity without significantly affecting printability. Samples 4 and 5, with 15 wt% and 20 wt% CF respectively, explore the upper bounds of fiber loading that remain processable via FFF without compromising filament continuity, nozzle clearance, or interlayer bonding.

Prior to compounding, both PETG pellets and carbon fibers were subjected to a drying process to eliminate moisture content, which could otherwise lead to polymer hydrolysis and poor print quality. Drying was conducted in a vacuum oven at 70 °C for 8 hours [28–30]. The dried constituents were then compounded using a twin-screw extruder operating at a temperature profile of 230–250 °C along the barrel and a screw speed of 60 rpm. The extrusion process ensured uniform dispersion of carbon fibers within the PETG matrix, producing composite filament strands of 1.75 mm diameter suitable for FFF. Twin-screw extrusion enables high shear mixing necessary to break agglomerates and distribute fibers evenly [31]. However, fiber attrition during processing must be minimized to retain the reinforcement benefits. The chosen extruder settings aim to balance shear for mixing with residence time control to prevent degradation of PETG and excessive fiber shortening.

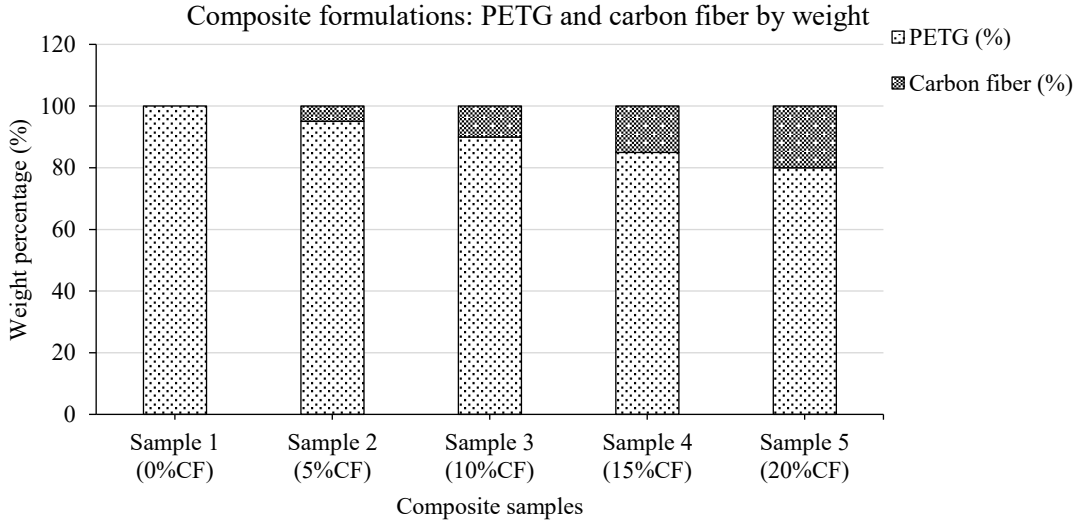

Figure 2. Weight percentage distribution of PETG and carbon fiber (CF) in five composite formulations.

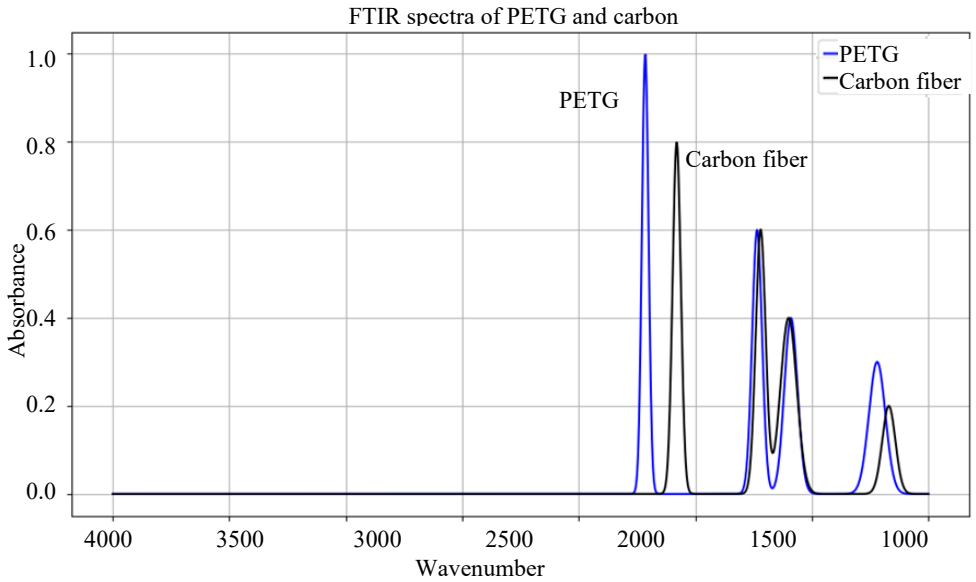

Figure 3. FTIR spectra of neat PETG and short carbon fiber (CF) over the range of 4000–500 cm^{-1}.

The extruded filaments were cooled using a calibrated water bath and subsequently passed through a laser diameter control system to ensure dimensional consistency. The filament was spooled and stored in sealed, desiccated containers prior to 3D printing to avoid moisture reabsorption [33].

Fourier Transform Infrared (FTIR) spectroscopy was employed to identify and confirm the functional groups present in the neat PETG and carbon fiber (CF) materials in the Figure 3. The FTIR spectrum of PETG revealed several characteristic absorption bands corresponding to its copolyester structure. A strong and sharp peak observed at approximately 1715 cm^{-1} corresponds to the C=O stretching vibration of ester groups, confirming the integrity of the polyester backbone. Additional peaks at around 1235 cm^{-1} and 1090 cm^{-1} are attributed to C-O and C-O-C stretching vibrations, respectively, while a weaker band near 720 cm^{-1} indicates aromatic ring out-of-plane deformations. These features are consistent with the expected chemical structure of PETG and confirm the presence of functional groups responsible for its thermal and mechanical properties.

The FTIR spectrum of carbon fiber, on the other hand, exhibited fewer peaks, reflecting its highly graphitized structure [34–35]. A prominent peak near 1580 cm^{-1} is associated with the aromatic C=C stretching vibration in the graphitic domains. Smaller peaks at approximately 1220 cm^{-1} and 1100 cm^{-1} suggest the presence of oxygen-containing functional groups such as epoxy or carboxyl groups likely introduced during fiber surface treatment to enhance matrix compatibility. A minor band observed near 670 cm^{-1} corresponds to out-of-plane ring deformation.

These spectral features confirm that the CF used in this study retains the graphitic character while also possessing surface functionality that could aid interfacial bonding with the PETG matrix [36]. The clear identification of these characteristic peaks in both materials indicates that no significant chemical degradation occurred during preprocessing or filament extrusion. Moreover, the retention of functional groups is critical for maintaining the mechanical integrity and interfacial adhesion within the composite system. This FTIR analysis establishes a foundational chemical understanding for further interpretation of mechanical and morphological results.

Filament Production

The PETG and carbon fiber composite filaments were fabricated in-house using a co-rotating twin-screw extruder designed for laboratory-scale compounding [37].

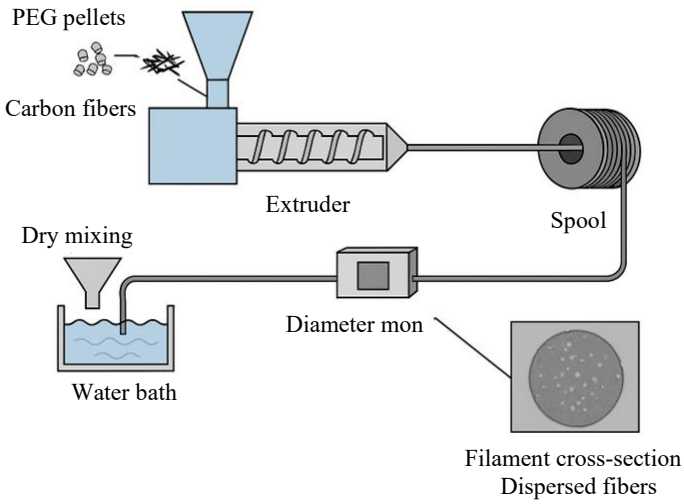

Figure 4. Schematic diagram of in-house filament production using a twin-screw extrusion setup.

Table 4. FFF Process parameters for CF-PETG composites.

Parameter	Value
Printer Model	Creality Ender 5 Pro
Extruder Type	Direct Drive
Nozzle Type	Hardened Steel
Nozzle Diameter	0.6 mm
Nozzle Temperature	245 ± 5 °C
Bed Temperature	80 °C
Printing Speed	40 mm/s
Layer Height	0.2 mm
Infill Density	100% (for mechanical tests)
Infill Pattern	Rectilinear (0°/90°)
Print Orientation	Flat XY-plane
Retraction Distance	2 mm
Retraction Speed	25 mm/s
Cooling Fan	Off (for PETG adhesion)

The process involved dry-blending PETG pellets with pre-dried short, chopped carbon fibers at prescribed weight percentages (10 wt% and 20 wt%), followed by melt compounding and filament extrusion. The extrusion was carried out using a Thermo Scientific™ Process 11 twin-screw extruder, configured with a screw diameter of 11 mm and an L/D ratio of 40:1 [38–39]. The barrel consisted of six independently controlled heating zones, with a temperature gradient maintained from 230°C at the hopper to 250°C at the die head, optimized to ensure uniform melting and fiber wetting while minimizing thermal degradation of the polymer. A screw speed of 60 rpm was used to balance shear-induced fiber dispersion with the risk of fiber breakage. The molten composite was extruded through a 1.75 mm diameter circular die and cooled immediately in a water bath, followed by air drying and inline dimensional monitoring using a laser micrometer to ensure consistent filament diameter (±0.05 mm tolerance). The filament was spooled and stored in vacuum-sealed desiccant bags to prevent moisture uptake. The Figure 4 shows the schematic diagram of in-house filament production using a twin-screw extrusion setup. PETG pellets and short chopped carbon fibers are dry-mixed, melt-compounded in a temperature-controlled extruder, extruded through a circular die, water-cooled, and wound into spools for FFF use. Inline diameter monitoring ensures dimensional consistency.

Table 4 summarizes the FFF process parameters used for all test samples. To ensure reliable and

consistent mechanical testing, all specimens were printed with 100% infill, effectively minimizing internal porosity and maximizing structural integrity. A rectilinear raster pattern at 0°/90° was employed to achieve uniform stress distribution under tensile and flexural loading. Cooling was intentionally disabled during printing to promote interlayer fusion, which is critical for PETG's bonding behavior due to its slow crystallization. Additionally, a hardened steel nozzle was used throughout to withstand abrasion from the carbon fiber reinforcement and maintain dimensional accuracy over extended print cycles.

FFF Parameters

All specimens were fabricated using a Creality Ender 5 Pro fused filament fabrication (FFF) 3D printer equipped with a direct drive extrusion system and a 0.6 mm hardened steel nozzle, selected specifically to handle the abrasive nature of carbon fiber–reinforced filaments [40–41]. Printing was performed on a heated glass bed maintained at 80 °C, while the nozzle temperature was set to 245 ± 5 °C to ensure consistent extrusion of both neat PETG and composite filaments. A layer height of 0.2 mm and printing speed of 40 mm/s were maintained throughout the study to balance resolution and deposition stability. The Figure 5 presents the core process parameters adopted during FFF-based fabrication of PETG and carbon fiber–reinforced PETG composites [42–43]. Specimens were printed in the flat XY-plane orientation, with layers deposited vertically along the Z-axis. A 100% infill density was used in all prints to eliminate void-induced variability and accurately assess the mechanical properties of the material. The infill pattern followed a 0°/90° rectilinear raster strategy, providing uniform internal reinforcement. Cooling fans were disabled during printing to promote stronger interlayer bonding, particularly beneficial for PETG, which bonds more effectively under slower cooling rates. Filament diameter was continuously monitored to ensure dimensional stability, and retraction settings were adjusted to minimize oozing and stringing between print paths.

Specimen Preparation

The specimens for mechanical testing were printed in accordance with established ASTM standards to ensure consistency and comparability of results. All samples were fabricated using the same FFF parameters outlined previously and were printed in the flat XY-plane orientation to minimize interlayer delamination and build-induced anisotropy. For tensile testing, Type I specimens were prepared in accordance with ASTM D638 [44], which is widely used for testing thermoplastic polymers. These specimens feature a standardized dog-bone shape with reduced cross-section in the gauge length to ensure uniform stress distribution during testing. Figure 6 illustrates the geometry of the ASTM D638 tensile specimen used in this study.

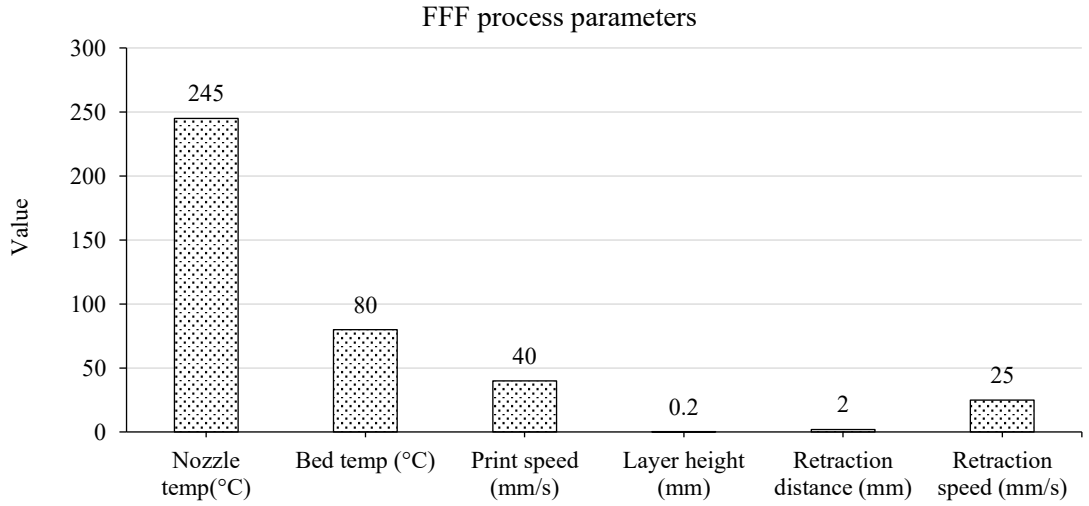

Figure 5. Key fused filament fabrication (FFF) process parameters used for printing PETG and CF-reinforced PETG composites.

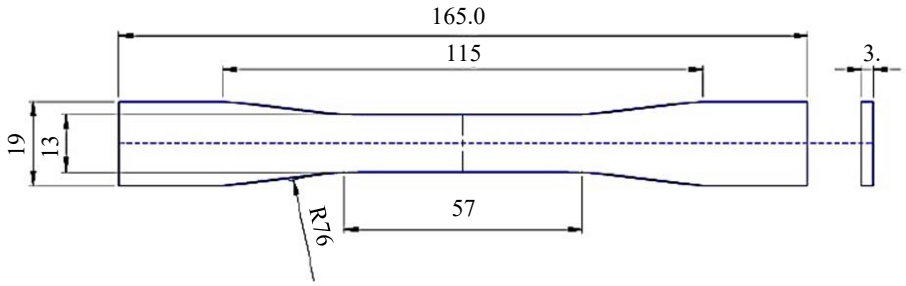

Figure 6. ASTM D638 Type I–Tensile testing specimen.

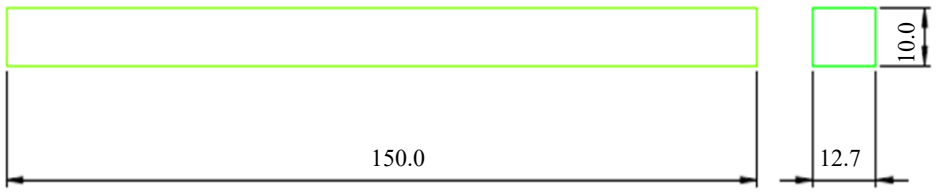

Figure 7. ASTM D790–Flexural testing specimen.

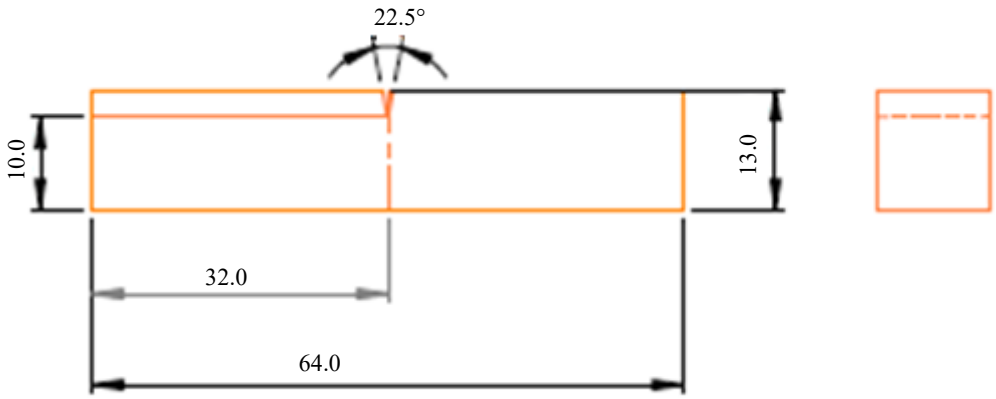

Figure 8. ASTM D256–Izod impact test specimen.

For flexural testing, rectangular bar specimens were printed following the guidelines of ASTM D790, suitable for three-point bending tests. This standard allows evaluation of flexural strength and modulus of materials under loading conditions that simulate bending in structural applications. Figure 7 shows the representative dimensions and profile of the ASTM D790 [45] flexural specimen.

For impact resistance evaluation, ASTM D256 (Izod impact) [46] was referenced, using notched specimens to assess energy absorption under high strain-rate conditions. Notches were precisely machined post-printing to maintain dimensional accuracy. Figure 8 depicts the ASTM D256 impact specimen, highlighting the notch geometry and dimensional compliance.

All samples were post-processed by light sanding of the edges to remove any burrs or imperfections. Dimensions were verified using a digital caliper, and samples with more than ±0.2 mm deviation from standard geometry were discarded. Prior to testing, specimens were conditioned at 23 ± 2 °C and $50 \pm 5\%$ RH for 48 hours in accordance with ASTM D618 to stabilize moisture content and ensure reliable data.

Characterization Techniques

To comprehensively evaluate the influence of carbon fiber reinforcement on PETG composites fabricated via fused filament fabrication (FFF), a series of characterization techniques were employed encompassing mechanical, thermal, and morphological analyses.

Mechanical Testing

Mechanical characterization involved tensile, flexural, and impact testing, each performed in accordance with relevant ASTM standards.

- Tensile testing was performed using a Tinius Olsen H50KS universal testing machine (50 kN load capacity) with an integrated extensometer. Testing followed ASTM D638 (Type I) at a crosshead speed of 5 mm/min, and provided tensile strength, Young's modulus, and elongation at break [47].
- Flexural testing was conducted on the same machine, configured with a three-point bending fixture as per ASTM D790, using a span length of 100 mm and a crosshead speed of 2 mm/min. Flexural strength and modulus were calculated based on load–deflection curves [48].
- Impact testing followed ASTM D256 (Izod method) using a Presto Izod/Charpy impact tester, with a 5.5 J hammer and digital readout. Notched specimens were tested to evaluate energy absorption under dynamic loading [49].

Each mechanical test was conducted on five replicates per formulation to ensure repeatability and statistical significance.

Thermal Characterization

Thermal behavior was assessed using the following instruments and protocols:

- Thermogravimetric Analysis (TGA) was carried out using a PerkinElmer TGA 4000 under nitrogen atmosphere, with samples heated from 30 °C to 600 °C at 10 °C/min. The test evaluated thermal stability, degradation onset temperature, and final residue (CF content) [50].
- Differential Scanning Calorimetry (DSC) analysis was conducted using a Mettler Toledo DSC 3+ instrument. Samples were heated from 25 °C to 250 °C at a rate of 10 °C/min under nitrogen, capturing glass transition temperature (Tg), potential crystallization, and melting events [51].
- Heat Deflection Temperature (HDT) was measured using a Ducom HDT/Vicat testing machine in accordance with ASTM D648. A standard load of 0.45 MPa was applied in an oil bath to assess the material's dimensional stability under heat and load [52].

Morphological Analysis

Fracture surface morphology was observed using Scanning Electron Microscopy (SEM) on a Carl Zeiss EVO 18 SEM, operated at an accelerating voltage of 15 kV. Samples (typically fractured tensile specimens) were gold-coated using a Quorum Q150R sputter coater to enhance conductivity prior to imaging [53–54]. SEM analysis was used to:

- Examine fiber orientation, dispersion, and possible agglomeration,
- Identify interlayer bonding quality and porosity,
- Characterize fracture mechanisms, distinguishing between brittle and ductile failure.
- These observations were correlated with mechanical test outcomes to better understand the structure–property relationships in the fabricated composites.

RESULTS AND DISCUSSION

Mechanical Properties

Mechanical characterization was conducted to evaluate the structural performance of PETG and PETG-carbon fiber (CF) composites under tensile, flexural, and impact loading. These tests provide insight into the reinforcement effects of CF and help identify the optimal fiber content for strength, stiffness, and toughness balance.

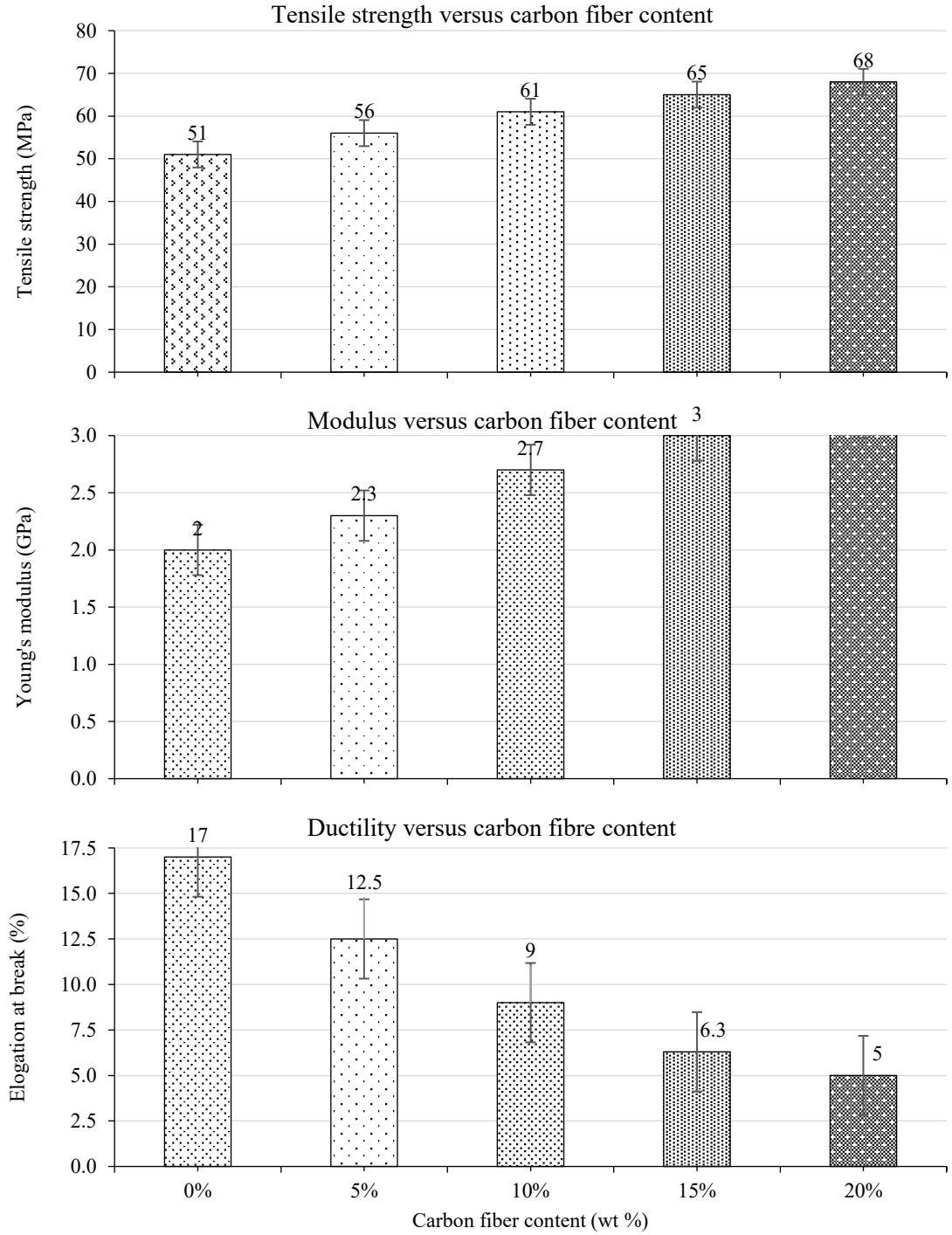

Figure 9. Mechanical properties of PETG–CF composites (mean ± SD, n=5).

Tensile Strength, Modulus, and Elongation at Break

The mechanical performance of PETG reinforced with varying carbon fiber (CF) contents (0–20 wt%) was evaluated via tensile testing, and the results are presented in Figure 9.

The figure highlights the progressive evolution of three key mechanical properties tensile strength, Young's modulus, and elongation at break as a function of CF loading. As observed, tensile strength increased from 51 MPa (0 wt% CF) to 68 MPa (20 wt% CF). This enhancement can be attributed to the

reinforcing role of carbon fibers, which provide load-bearing capacity and restrict polymer chain mobility under stress. The Young's modulus also showed a consistent rise, from 2.0 GPa to 3.2 GPa, confirming increased stiffness due to the intrinsic rigidity of the CF inclusions and improved interfacial adhesion. On the other hand, ductility, as measured by elongation at break, decreased sharply from 17% to 5%. This inverse trend suggests a trade-off between strength and flexibility, as the brittle nature of CF particles constrains the matrix's plastic deformation. The error bars (mean ± SD, n=5) indicate low variability across specimens, confirming consistent printing and testing conditions. Together, the data suggest that moderate CF loading (10-15 wt%) offers an optimal balance of mechanical strength and structural reliability without excessively compromising flexibility.

Flexural Strength and Modulus

The flexural performance of PETG-CF composites was assessed using three-point bending tests as per ASTM D790 standards. The results, depicted in Figure 10, demonstrate a clear improvement in both flexural strength and flexural modulus with increasing carbon fiber (CF) content. Neat PETG (0 wt% CF) exhibited a baseline flexural strength of 78 MPa and a modulus of 2.1 GPa. With the introduction of 5 wt% CF, strength increased to 88 MPa, and modulus rose to 2.6 GPa. The mechanical benefits continued with higher fiber loadings, reaching 112 MPa strength and 3.7 GPa modulus at 20 wt% CF.

This trend reflects the inherent stiffness of carbon fibers and their effective reinforcement within the PETG matrix, which restricts deformation under bending stress. Notably, the improvements in modulus were more gradual than tensile properties, indicating that flexural stiffness is more sensitive to fiber distribution and alignment across the sample cross-section. The small standard deviations confirm reproducibility and uniformity in specimen fabrication and testing. These results affirm the suitability of CF reinforcement for structural applications where flexural rigidity is critical, especially in parts subjected to bending loads such as brackets, enclosures, and housings.

Impact Resistance (Izod Notched)

The impact resistance of PETG–CF composites was assessed using Izod notched impact tests in accordance with ASTM D256 standards. The results, summarized in the Figure 11, indicate a consistent decline in impact strength with increasing carbon fiber (CF) content. Neat PETG (0 wt%) exhibited the highest energy absorption at 36 kJ/m², owing to its inherent ductility and ability to undergo significant plastic deformation under high-strain loading. As CF content increased to 5, 10, 15, and 20 wt%, the impact strength decreased progressively to 29, 24, 19, and 15 kJ/m², respectively.

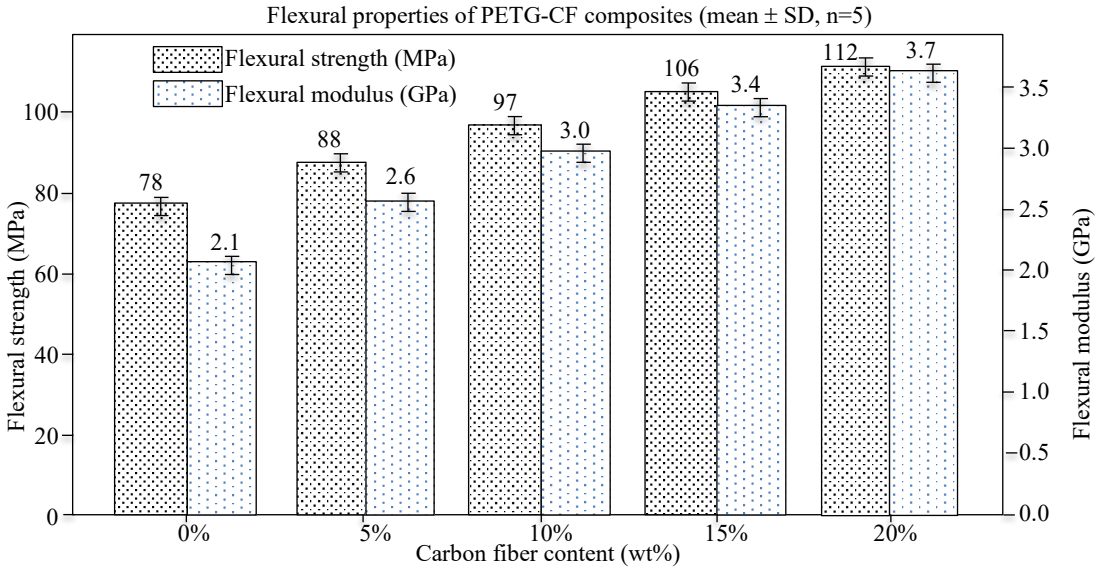

Figure 10. Flexural strength and modulus of PETG–CF composites across various carbon fiber weight percentages (mean ± SD, n=5).

This downward trend is attributed to the brittle nature of carbon fibers and the increased stiffness they introduce into the polymer matrix. While CFs enhance tensile and flexural performance, they limit the polymer's ability to deform plastically during impact, thereby reducing toughness.

Additionally, the presence of CFs introduces potential crack initiation sites, especially at the fiber–matrix interfaces, which act as stress concentrators under rapid loading conditions. Despite the reduction in impact resistance, the composites remain viable for moderately dynamic applications where mechanical strength is prioritized over toughness.

Effect of Carbon Fiber Content

The Figure 12 presents a comparative trend analysis of the key mechanical properties tensile strength, flexural strength, and impact resistance as a function of carbon fiber (CF) content (0–20 wt%) in PETG composites. This multi-property perspective highlights the trade-offs and optimization windows inherent in fiber-reinforced polymer systems. As CF loading increased, both tensile and flexural strength exhibited a near-linear enhancement. Tensile strength rose from 51 MPa (0 wt%) to 68 MPa (20 wt%), while flexural strength improved more markedly from 78 MPa to 112 MPa over the same range. These gains reflect the high modulus of carbon fibers and their ability to restrict matrix deformation, leading to superior stress transfer and load-bearing efficiency.

The flexural strength demonstrated steeper improvement, attributed to the fact that bending loads engage the full cross-section of the composite, thus amplifying the influence of embedded fibers. Conversely, impact strength decreased consistently with rising CF content, falling from 36 kJ/m² to 15 kJ/m². This behavior is characteristic of short-fiber composites, where stiff reinforcements hinder matrix ductility and initiate stress concentrations at the fiber–matrix interface. The reduction in impact resistance underscores the brittle shift in fracture behavior at higher fiber loadings, a critical consideration for dynamically loaded applications.

The 10-15 wt% CF window emerges as a practical compromise, delivering substantial stiffness and strength improvements while maintaining acceptable ductility and toughness. Beyond 15 wt%, mechanical gains begin to plateau, and brittleness becomes more pronounced, suggesting diminishing returns in mechanical reinforcement efficiency.

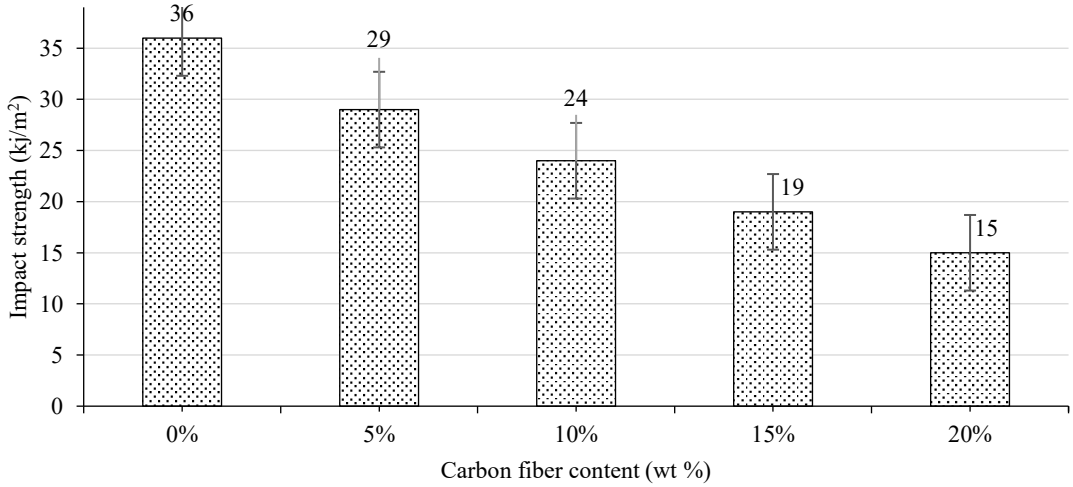

Figure 11. Izod notched impact strength of PETG–CF composites across varying carbon fiber contents (mean ± SD, n=5).

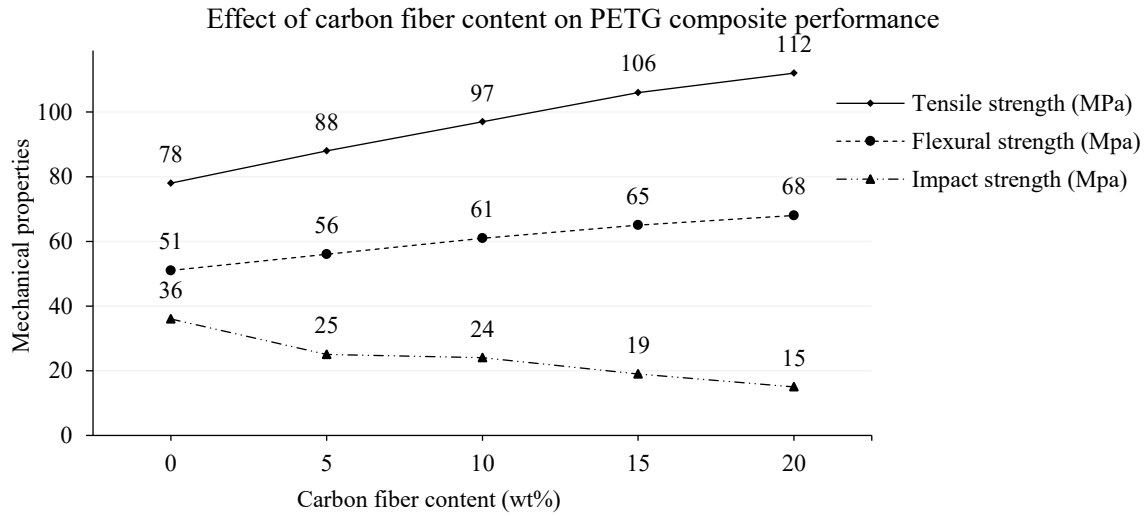

Figure 12. Effect of carbon fiber content (0-20 wt%) on the tensile strength, flexural strength, and impact resistance of PETG composites.

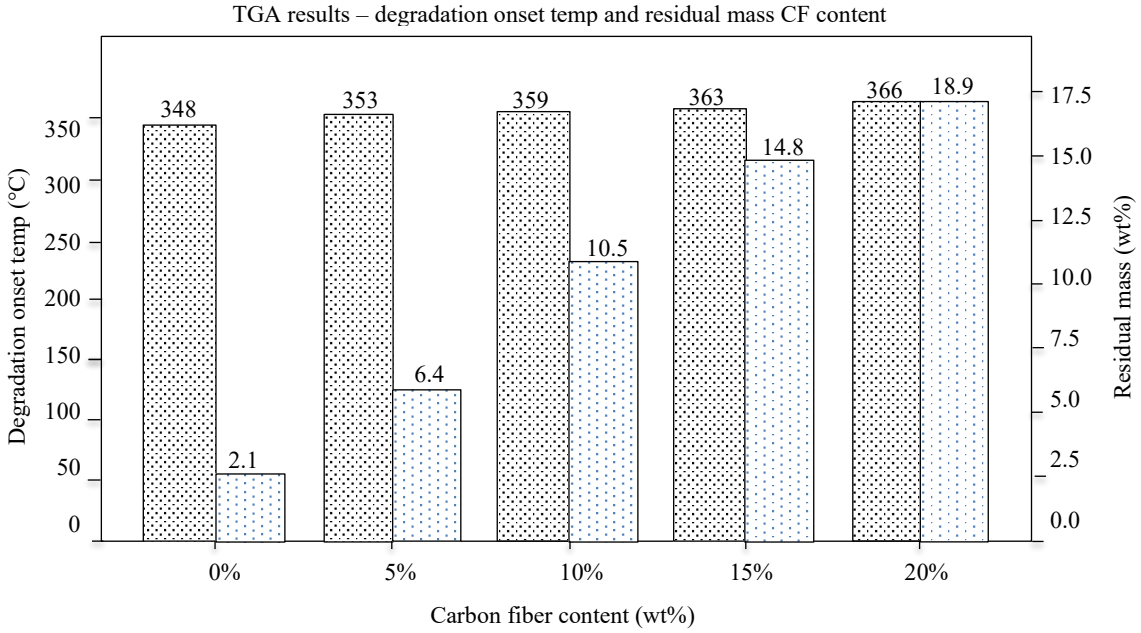

Figure 13. TGA results showing the variation in degradation onset temperature and residual mass with increasing carbon fiber (CF) content in PETG composites.

Thermal Properties

The thermal behavior of PETG and its carbon fiber (CF)-reinforced composites was investigated to evaluate their suitability for applications requiring elevated thermal resistance. A combination of thermogravimetric analysis (TGA), differential scanning calorimetry (DSC), and heat deflection temperature (HDT) testing was performed to understand the degradation characteristics, thermal transitions, and stability under load.

TGA Results – Thermal Stability Enhancement

Thermogravimetric analysis (TGA) was conducted to assess the thermal degradation behavior and char yield of the PETG-CF composites. As illustrated in the Figure 13, the degradation onset temperature increased progressively from 348 °C for neat PETG to 366 °C for the 20 wt% CF

composites. This enhancement indicates that the carbon fiber reinforcement acts as a thermal barrier, delaying the volatilization of the matrix by impeding heat flow and degradation propagation. Simultaneously, the residual mass at 600 °C increased significantly from 2.1 wt% to 18.9 wt%, confirming the higher thermal stability and inert nature of the CF phase, which remains undecomposed under oxidative conditions. The increase in char yield is also advantageous in applications demanding flame retardancy or high-temperature resistance.

Together, these results suggest that CF addition not only reinforces mechanical strength but also enhances the thermal degradation resistance of PETG, making the material more viable for thermally demanding applications such as structural components and heat-exposed enclosures.

DSC Results – Thermal Transitions and Crystallinity

Differential scanning calorimetry (DSC) was performed to evaluate the thermal transitions of the composites, particularly the glass transition temperature (Tg) and crystallinity. As shown in Figure 14, the Tg increased gradually from 81.5 °C for neat PETG to 83.6 °C at 20 wt% CF. This shift suggests a restriction of polymer chain mobility due to the presence of rigid carbon fibers, which hinder segmental motion within the matrix. In parallel, the degree of crystallinity exhibited a rising trend, increasing from 7.2% to 10.8% as CF content increased. The carbon fibers likely act as heterogeneous nucleating agents during cooling, promoting localized crystalline region formation in the PETG matrix. These results confirm that CF incorporation not only strengthens the composite mechanically but also influences its thermal transition behavior, improving dimensional stability and structural integrity in temperature-sensitive applications.

Heat Deflection Temperature (HDT)

Heat deflection temperature (HDT) is a critical metric for evaluating a polymer's ability to maintain its shape and mechanical integrity under elevated temperatures and load. As illustrated in Figure 15, HDT showed a clear upward trend with increasing carbon fiber (CF) content, ranging from 70 °C for neat PETG to 83 °C for 20 wt% CF. This enhancement in thermal stability is primarily attributed to the incorporation of rigid carbon fibers into the PETG matrix, which restricts polymer chain movement and delays the onset of softening under thermal stress.

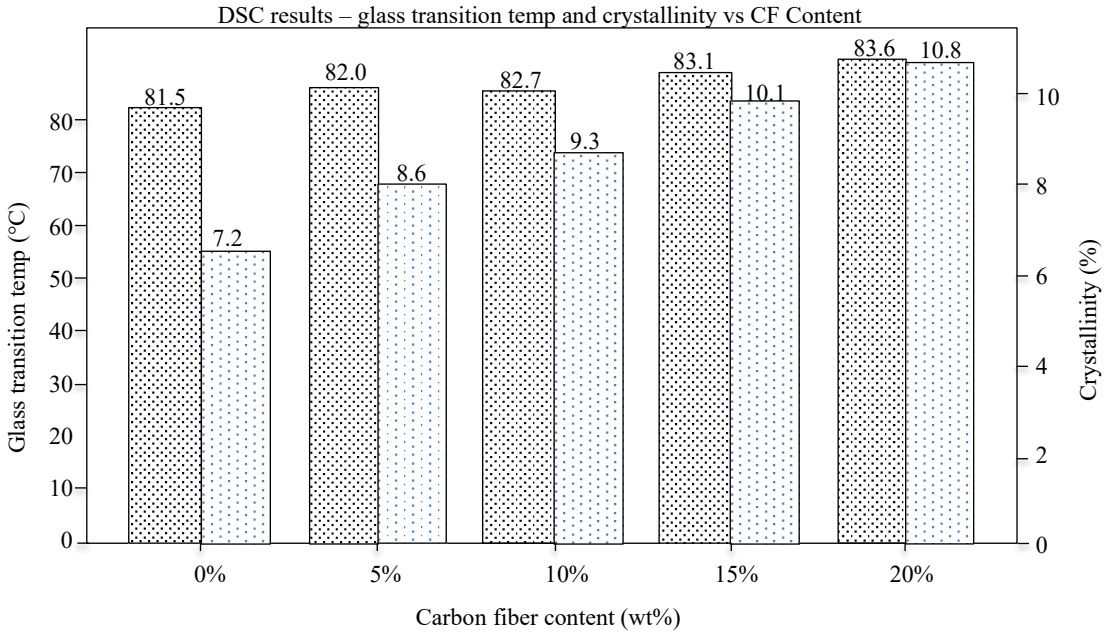

Figure 14. Influence of carbon fiber content on the glass transition temperature (Tg) and crystallinity of PETG-CF composites.

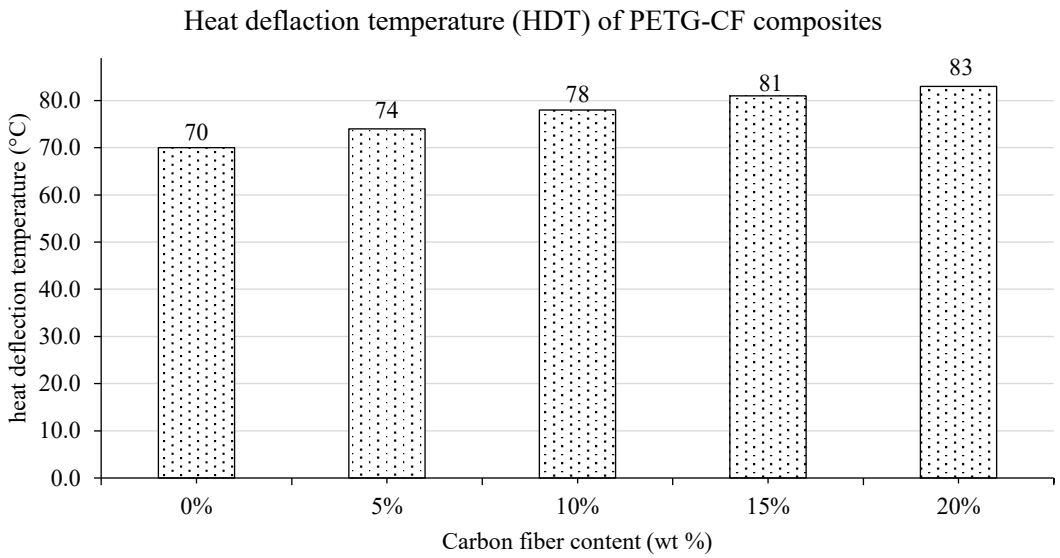

Figure 15. Heat deflection temperature (HDT) of PETG–CF composites.

As the fiber loading increases, the composite's overall stiffness improves, translating into greater resistance to deformation at elevated temperatures. The gain in HDT is particularly valuable for applications involving continuous thermal exposure or cyclic heating, such as housings, structural brackets, or components in engine bays and electronics. Notably, while the increase from 10% to 20% CF shows a gradual HDT improvement, the rate of gain begins to plateau, suggesting an approach toward a reinforcement saturation point. These findings align well with the trends observed in the dynamic mechanical analysis (DMA), reinforcing that CF reinforcement not only improves mechanical stiffness but also boosts the material's thermal endurance envelope.

SEM Analysis of Fracture Surfaces at Varying Carbon Fiber Loadings

The Figure 16 presents scanning electron micrographs of the fracture surfaces of PETG–CF composites with varying carbon fiber (CF) loadings, offering insights into the evolving microstructure and interfacial characteristics. At 0 wt% CF, neat PETG (Figure 16a) exhibits a relatively smooth and homogeneous fracture surface, characteristic of ductile failure behavior. The absence of reinforcement, micro-voids, or notable defects confirms a uniform polymer morphology. Distinct FFF layer lines are visible, but with no interfacial delamination, suggesting strong intra-layer adhesion under the optimized print parameters.

With the addition of 5 wt% CF (Figure 16b), dispersed short carbon fibers become visible, partially aligned with the print path. The fibers appear well embedded in the matrix, with only minor voids forming around some peripheries, indicating localized fiber-matrix debonding. The reinforcement appears to be effectively distributed at this level, with minimal disruption to the base polymer.

At 10 wt% CF (Figure 16c), the composite shows a denser and more uniform dispersion of CF throughout the matrix. The fibers are embedded without significant pull-out or debonding, suggesting excellent interfacial bonding. The surface morphology remains stable, with minimal evidence of microstructural defects, confirming efficient stress transfer between matrix and reinforcement. However, at 15 wt% CF (Figure 16d), partial fiber agglomeration becomes evident. Overlapping and misaligned fibers lead to localized clustering and the emergence of fiber-rich domains. While interlayer fusion appears mostly preserved, these clusters introduce micro-voids and inhomogeneities that may affect mechanical consistency and reliability. Finally, the 20 wt% CF sample (Figure 16€) shows clear signs of pronounced agglomeration, with dense fiber bundles disrupting the polymer continuity.

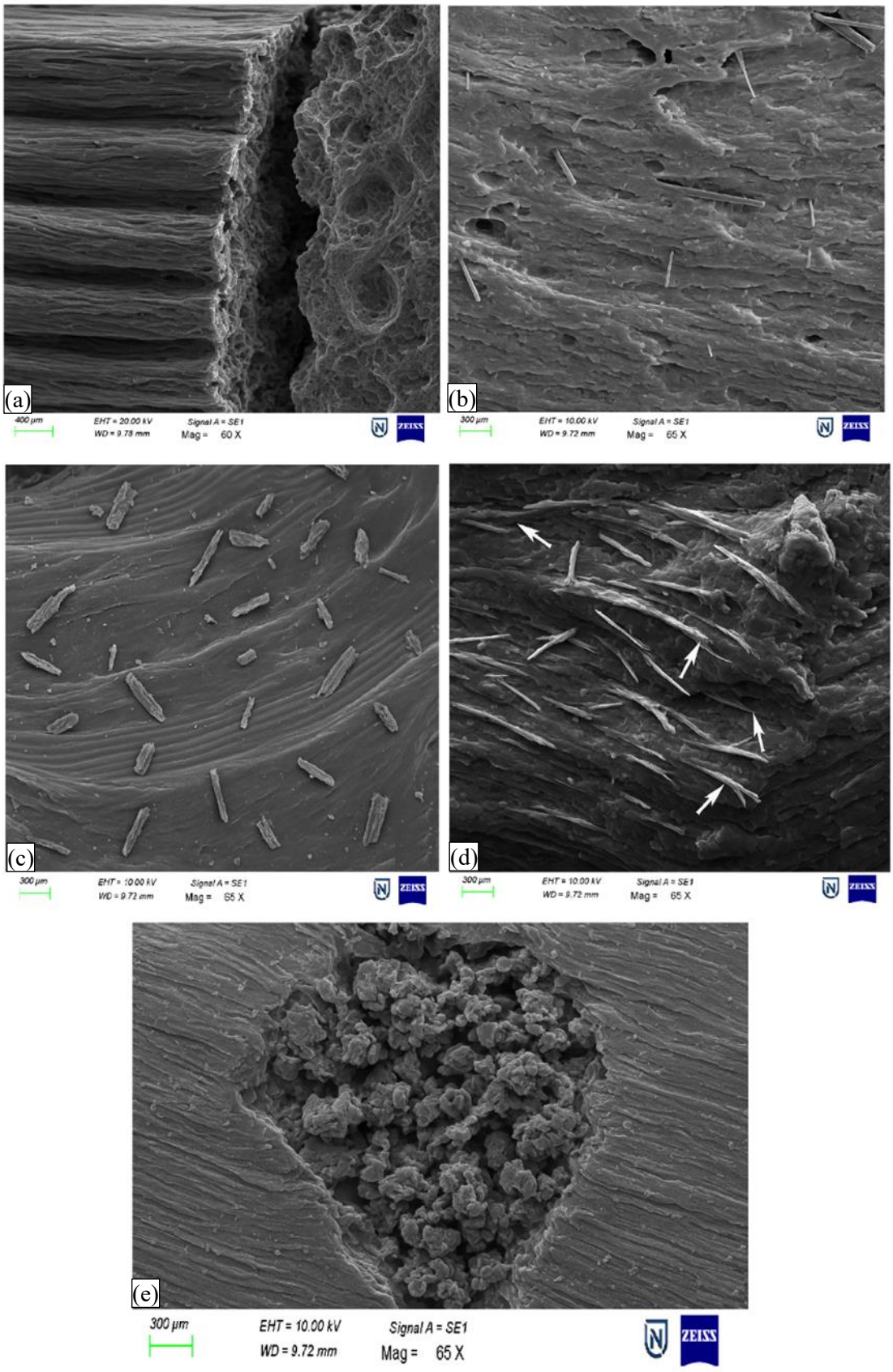

Figure 16. SEM Micrographs of PETG-CF composites at varying CF loadings.

These concentrated clusters of CF introduce stress concentration points and matrix–fiber debonding zones, likely contributing to decreased ductility and greater brittleness. While mechanical stiffness may benefit from higher fiber content, the SEM images reflect the trade-off in terms of dispersion quality and interfacial stress distribution.

CONCLUSIONS

The study comprehensively investigated the fabrication and characterization of PETG–carbon fiber (CF) composites using the Fused Filament Fabrication (FFF) method, focusing on the influence of short CF reinforcement on mechanical, thermal, and morphological behavior. Composite formulations were prepared with CF contents ranging from 0 to 20 wt%, and specimens were fabricated under standardized FFF processing parameters to ensure reproducibility and comparability. The results demonstrated that the addition of CF significantly enhanced the performance of PETG across key functional domains. At 20 wt% CF loading, tensile strength increased from ~51 MPa (neat PETG) to ~68 MPa (+33%), and Young's modulus improved from ~2.0 GPa to ~3.2 GPa (+60%). Similarly, flexural strength and modulus rose by 44% and 76%, respectively, reaching 112 MPa and 3.7 GPa. Thermal performance was also bolstered, with the heat deflection temperature (HDT) increasing from 70 °C to 83 °C, and the glass transition temperature (Tg) shifting from 81.5 °C to 83.6 °C. These enhancements were attributed to effective stress transfer, improved interfacial bonding, and the nucleating effect of CF within the PETG matrix. Morphological analysis via SEM revealed excellent fiber dispersion up to 10 wt% CF, while higher loadings (≥15 wt%) introduced agglomeration, microvoids, and potential interfacial defects. Printability remained stable at lower CF contents, but challenges such as nozzle clogging, surface roughness, and warping became apparent at 20 wt% CF, necessitating hardened nozzles and refined print settings. Despite the mechanical and thermal gains, a marked reduction in ductility was observed, with elongation at break falling from ~17% to ~5%, underscoring the brittleness induced by excessive fiber loading. Therefore, a balance around 10–15 wt% CF may offer an optimal trade-off between stiffness and toughness for practical applications. In terms of applicability, the reinforced PETG composites exhibit properties suitable for engineering applications such as functional brackets, automotive interiors, UAV components, and structural fixtures where moderate-to-high rigidity and thermal resilience are essential.

Acknowledgments

The authors express their sincere gratitude to Nitte (Deemed to be University), Nitte Meenakshi Institute of Technology (NMIT), Bengaluru, Karnataka, for providing the necessary facilities and support for conducting this research. Special thanks to the Department of Mechanical Engineering for their valuable guidance and encouragement throughout the study. The authors also acknowledge the contributions of research scholars and laboratory staff for their assistance in experimental analysis and data collection.

REFERENCES

1. Wypych, G. Handbook of Polymers; Elsevier: Amsterdam, Holland, 2016.
2. F.A. Santos, H. Rebelo, M. Coutinho, L.S. Sutherland, C. Cismasiu, I. Farina, F. Fraternali, Low velocity impact response of 3D printed structures formed by cellular metamaterials and stiffening plates: PLA vs. PETG, Compos. Struct. 256 (2021), 113128.
3. E. Provaggi, C. Capelli, B. Rahmani, G. Burriesci, D.M. Kalaskar, 3D printing assisted finite element analysis for optimising the manufacturing parameters of a lumbar fusion cage, Mater. Des. 163 (2019), 107540.
4. V. Mahesh, Experimental investigation on the dynamic response of additive manufactured PETG composite beams reinforced with organically modified montmorillonite nanoclay and short carbon fiber, Polym. Compos. 42 (10) (2021) 5021–5034.
5. I. Blanco, The use of composite materials in 3D printing, J. Compos. Sci. 4 (2) (2020) 42.

6. I.M. Alarifi, Investigation of the dynamic mechanical analysis and mechanical response of 3D printed nylon carbon fiber composites with different build orientation, Polym. Compos. 43 (8) (2022) 5353–5363.
7. S.H. Borujeni, S.Z. Mirdamadian, J. Varshosaz, A. Taheri, Three-dimensional (3D) printed tablets using ethyl cellulose and hydroxypropyl cellulose to achieve zero order sustained release profile, Cellulose 27 (3) (2020) 1573–1589.
8. K. Szykiedans, W. Credo, D. Osiński, Selected mechanical properties of PETG 3-D prints, Procedia Eng. 177 (2017) 455–461.
9. G.J. Bex, B.L. Ingenhut, T. ten Cate, M. Sezen, G. Ozkoc, Sustainable approach to produce 3D-printed continuous carbon fiber composites: "A comparison of virgin and recycled PETG," Polym. Compos. 42 (9) (2021) 4253–4264.
10. H.R. Vanaei, S. Khelladi, M. Deligant, M. Shirinbayan, A. Tcharkhtchi, Numerical prediction for temperature profile of parts manufactured using fused filament fabrication, J. Manuf. Process. 76 (2022) 548–558.
11. M. Sadia, A. Sośnicka, B. Arafat, A. Isreb, W. Ahmed, A. Kelarakis, M.A. Alhnan, Adaptation of pharmaceutical excipients to FDM 3D printing for the fabrication of patient-tailored immediate release tablets, Int. J. Pharm. 513 (1–2) (2016) 659–668.
12. R.T.L. Ferreira, I.C. Amatte, T.A. Dutra, D. Bürger, Experimental characterization and micrography of 3D printed PLA and PLA reinforced with short carbon fibers, Compos. B Eng. 124 (2017) 88–100.
13. M. Kucewicz, P. Baranowski, J. Małachowski, A method of failure modeling for 3D printed cellular structures, Mater. Des. 174 (2019), 107802.
14. U.K. Komal, B.K. Kasaudhan, I. Singh, Comparative performance analysis of polylactic acid parts fabricated by 3D printing and injection molding, J. Mater. Eng. Perform. (2021) 1–7.
15. M. Kováčová, J. Kozakovičová, M. Procházka, I. Janigová, M. Vysopal, I. Černičková, J. Krajčovič, Z. Špitalský, Novel hybrid PETG composites for 3D printing, Appl. Sci. 10 (9) (2020) 3062.
16. G. Dolzyk, S. Jung, Tensile and fatigue analysis of 3D-printed polyethylene terephthalate glycol, J. Fail. Anal. Prev. 19 (2) (2019) 511–518.
17. M. Chapiro, Current achievements and future outlook for composites in 3D printing, Reinforc Plast 60 (6) (2016) 372–375.
18. A. Kulkarni, G.D. Sorarù, J.M. Pearce, Polymer-derived SiOC replica of material extrusion-based 3-D printed plastics, Addit. Manuf. 32 (2020), 100988.
19. N. Vidakis, M. Petousis, L. Tzounis, E. Velidakis, N. Mountakis, S.A. Grammatikos, Polyamide 12/multiwalled carbon nanotube and carbon black nanocomposites manufactured by 3D printing fused filament fabrication: a comparison of the electrical, thermoelectric, and mechanical properties, Chimia 7 (2) (2021) 38.
20. B.G. Thiam, A. El Magri, H.R. Vanaei, S. Vaudreuil, 3D printed and conventional membranes - a review, Polymers 14 (5) (2022) 1023.
21. M.A.B. Helú, L. Liu, Fused deposition modeling (FDM) based 3D printing of microelectrodes and multi-electrode probes, Electrochim. Acta 365 (2021) 137279.
22. N. Bossa, J.M. Sipe, W. Berger, K. Scott, A. Kennedy, T. Thomas, C.O. Hendren, M. R. Wiesner, Quantifying Mechanical Abrasion of MWCNT Nanocomposites used in 3D Printing: influence of CNT content on abrasion products and rate of microplastic production, Environ. Sci. Technol. 55 (15) (2021) 10332–10342.
23. Y. Wang, M. Lei, Q. Wei, Y. Wang, J. Zhang, Y. Guo, J. Saroia, 3D printing biocompatible l-Arg/GNPs/PLA nanocomposites with enhanced mechanical property and thermal stability, J. Mater. Sci. 55 (12) (2020) 5064–5078.
24. D.M. Sánchez, M. de la Mata, F.J. Delgado, V. Casal, S.I. Molina, Development of carbon fiber acrylonitrile styrene acrylate composite for large format additive manufacturing, Mater. Des. 191 (2020), 108577.

25. A. Hamidi, Y. Tadesse, Single step 3D printing of bioinspired structures via metal reinforced thermoplastic and highly stretchable elastomer, Compos. Struct. 210 (2019) 250–261.
26. D. Jiang, D.E. Smith, Anisotropic mechanical properties of oriented carbon fiber filled polymer composites produced with fused filament fabrication, Addit. Manuf. 18 (2017) 84–94.
27. A.F. Kichloo, A. Raina, M.I.U. Haq, M.S. Wani, Impact of carbon fiber reinforcement on mechanical and tribological behavior of 3D-printed polyethylene terephthalate glycol polymer composites - an experimental investigation, J. Mater. Eng. Perform. (2021) 1–18.
28. P. Latko-Durałek, K. Dydek, A. Boczkowska, Thermal, rheological and mechanical properties of PETG/RPETG blends, J. Polym. Environ. 27 (11) (2019) 2600–2606.
29. P.P. Agarwal, T.S. Dadmode, M.R. Kadav, A.P. Ogale, P.P. Mangave, Experimental analysis of mechanical properties of PETG material 3D printed material by using fused deposition modelling technique, J. Mech. Mech. Eng. 6 (2020) 20–27.
30. E. García, P.J. Núñez, M.A. Caminero, J.M. Chacón, S. Kamarthi, Effects of carbon fibre reinforcement on the geometric properties of PETG-based filament using FFF additive manufacturing, Compos. B Eng. 235 (2022), 109766.
31. R. Srinivasan, K.N. Kumar, A.J. Ibrahim, K.V. Anandu, R. Gurudhevan, Impact of fused deposition process parameter (infill pattern) on the strength of PETG part, Mater. Today Proc. 27 (2020) 1801–1805.
32. B. Lepoittevin, P. Roger, Poly (ethylene terephthalate), Handb. Eng. Special. Thermoplastics 3 (2011) 97–126.
33. K.S. Erokhin, E.G. Gordeev, V.P. Ananikov, Revealing interactions of layered polymeric materials at solid-liquid interface for building solvent compatibility charts for 3D printing applications, Sci. Rep. 9 (1) (2019) 1–14.
34. M.T. Sepahi, H. Abusalma, V. Jovanovic, H. Eisazadeh, Mechanical properties of 3D-printed parts made of polyethylene terephthalate glycol, J. Mater. Eng. Perform. 30 (9) (2021) 6851–6861.
35. S. Kasmi, G. Ginoux, S. Allaoui, S. Alix, Investigation of 3D printing strategy on the mechanical performance of coextruded continuous carbon fiber reinforced PETG, J. Appl. Polym. Sci. 138 (37) (2021), 50955.
36. M.H. Hsueh, C.J. Lai, S.H. Wang, Y.S. Zeng, C.H. Hsieh, C.Y. Pan, W.C. Huang, Effect of printing parameters on the thermal and mechanical properties of 3D-printed PLA and PETG, using fused deposition modeling, Polymers 13 (11) (2021) 1758.
37. A. İpekçi, B. Ekici, Effect of fiber set-up and density on mechanical behavior of robotic 3D-printed composites, Emerg. Mater. Res. 11 (1) (2021) 160–166.
38. M. Kam, A. İpekçi, Ö. Şengül, Effect of FDM process parameters on the mechanical properties and production costs of 3D printed PowerABS samples, Int. J. Anal. Exp. Finite Element Anal. 7 (3) (2020) 77–90.
39. M.S. Srinidhi, R. Soundararajan, K.S. Satishkumar, S. Suresh, Enhancing the FDM infill pattern outcomes of mechanical behavior for as-built and annealed PETG and CFPETG composites parts, Mater. Today Proc. 45 (2021) 7208–7212.
40. N. Vidakis, M. Petousis, E. Velidakis, M. Liebscher, V. Mechtcherine, L. Tzounis, On the strain rate sensitivity of fused filament fabrication (FFF) processed PLA, ABS, PETG, PA6, and PP thermoplastic polymers, Polymers 12 (12) (2020) 2924.
41. S. Guessasma, S. Belhabib, H. Nouri, Printability and tensile performance of 3D printed polyethylene terephthalate glycol using fused deposition modelling, Polymers 11 (7) (2019) 1220.
42. K. Hibbert, G. Warner, C. Brown, O. Ajide, G. Owolabi, A. Azimi, The effects of build parameters and strain rate on the mechanical properties of FDM 3D-Printed acrylonitrile Butadiene Styrene, Open J. Org. Polym. Mater. 9 (2019) 1, 01.
43. A. İpekçi, B. Ekici, Experimental and statistical analysis of robotic 3D printing process parameters for continuous fiber reinforced composites, J. Compos. Mater. 55 (19) (2021) 2645–2655.
44. Alarifi, I. M. (2023). Polymer Testing, 120, 107949. https://doi.org/10.1016/j.polymertesting.2023.107949

45. Alarifi, I. M. (2020). Polymer Testing, 84, 106392. https://doi.org/10.1016/j.polymertesting.2020.106392
46. Alarifi, I. M. (2023). Journal of Materials Research and Technology, 23, 656–669. https://doi.org/10.1016/j.jmrt.2023.01.043
47. Pérez-Mendoza, G. J., et al. (2023). Microscopy and Microanalysis, 29, 1447–1449. https://doi.org/10.1093/micmic/ozad067.744
48. Böhme, T., et al. (2023). Microscopy and Microanalysis, 29, 212–218. https://doi.org/10.1093/micmic/ozac007
49. Li, W., et al. (2023). Textile Research Journal, 93, 1005–1018. https://doi.org/10.1177/004051752211260
50. Tarfaoui, M., et al. (2024). Composites Science and Technology, 247, 110385. https://doi.org/10.1016/j.compscitech.2023.110385
51. I.M. Alarifi, A performance evaluation study of 3D printed nylon/glass fiber and nylon/carbon fiber composite materials, J. Mater. Res. Technol. 21 (2022) 884–892.
52. T.D. Harpool, I.M. Alarifi, B.A. Alshammari, A. Aabid, M. Baig, R.A. Malik, A. Mohamed Sayed, R. Asmatulu, T.M.A.A. El-Bagory, Evaluation of the infill design on the tensile response of 3D printed polylactic acid polymer, Materials 14 (9) (2021) 2195.
53. J. Song, Q. Yuan, H. Zhang, B. Huang, F. Fu, Elevated conductivity and electromagnetic interference shielding effectiveness of PVDF/PETG/carbon fiber composites through incorporating carbon black, J. Polym. Res. 22 (8) (2015) 1–8.
54. H.A. Santana, N.S.A. Júnior, D.V. Ribeiro, M.S. Cilla, C.M. Dias, 3D printed mesh reinforced geopolymer: notched prism bending, Cement Concr. Compos. 116 (2021) 103892.

